Gene 822 (2022) 146346

Contents lists available at ScienceDirect

Gene

journal homepage: www.elsevier.com/locate/gene

Research paper

# Transcriptomic and functional studies reveal miR-431-5p as a tumour suppressor in pancreatic ductal adenocarcinoma cells

Øyvind P. Haugen [a,*,1], Cuong Khuu [a], Hanne M. Weidemann [a], Tor Paaske Utheim [a,b], Linda Hildegard Bergersen [a]

[a] Institute of Oral Biology, Faculty of Dentistry, University of Oslo, P.O. Box 1052 Blindern, 0316 Oslo, Norway
[b] Department of Medical Biochemistry, Oslo University Hospital, P.O. Box 4950 Nydalen, 0424 Oslo, Norway

ARTICLE INFO

Edited by: John Doe

*Keywords:*
Pancreatic cancer
PDAC
miRNA
mRNA sequencing
Apoptosis
Tumour suppressor

ABSTRACT

The lactate receptor HCAR1 (hydroxycarboxylic acid receptor 1) is highly expressed in pancreatic ductal adenocarcinoma (PDAC), where it regulates lactate transport between the cancer cells. Little is known about the underlying cause of high *HCAR1* expression in PDAC, and in the present study, we investigated whether *HCAR1* could be a target of miRNA regulation. By searching for predicted miRNA candidates *in silico*, we identified miR-431-5p as a possible regulator of *HCAR1*. We found miR-431-5p to repress *HCAR1* expression through direct binding to the 3′ UTR. The endogenous expression of miR-431-5p and *HCAR1* was found to be negatively related in the PDAC cell lines BxPC-3, Capan-2, and PANC-1. Overexpression of miR-431-5p inhibited cell proliferation in all the cell lines, and a shift in cell cycle progression and induction of apoptosis were found in the BxPC-3 cells. Transcriptomic analysis of mRNA from BxPC-3 cells revealed numerous differentially expressed genes (DEGs), including *HCAR1*, in response to miR-431-5p overexpression. A significant proportion of these DEGs was enriched in cancer-related processes and signalling pathways. Among the most significantly repressed DEGs was *ATP6V0E1*, encoding the integral subunit e of vacuolar ATPase (V-ATPase), an enzyme that is important for cancer cell survival. Small interfering RNA (siRNA)-mediated knockdown of *HCAR1* and *ATP6V0E1* showed that only knockdown of *ATP6V0E1* mimicked the effect of miR-431-5p overexpression on cell viability. Our findings indicate that miR-431-5p acts as a tumour suppressor in PDAC cells, with BxPC-3 cells being most responsive.

## 1. Introduction

Pancreatic cancer (PC) is a malignancy with poor prognosis (Bray et al., 2018). In contrast to the increased survival rate of most cancers, the survival rate for PC has barely changed for decades. Patients have an expected 5-year relative survival rate of only 9%, mainly due to late diagnosis and inefficient treatment options (Siegel et al., 2020). According to 2018 GLOBOCAN estimates, PC is the fourth leading cause of cancer-related death in the Western world and seventh worldwide (https://gco.iarc.fr/). With the current trend, PC is expected to become the second leading cause of cancer-related death in the US before 2030 (Rahib et al., 2014). Due to only modest improvements in recent treatments, there is an urgent need for discovering new biomarkers and therapies.

Pancreatic ductal adenocarcinoma (PDAC) accounts for the large majority of PC cases (Kleeff et al., 2016). As tumours grow, they become poorly vascularized and thus contain areas with varying levels of oxygen. PDAC tumours are particularly hypoxic, and the adaptation to a limited oxygen supply renders PDAC cells resistant to conventional chemo- and radiotherapy and promotes a metastatic phenotype (Erkan et al., 2016). To compensate for the lack of adequate oxygen levels, cells in hypoxic regions reprogram their metabolism and become predominantly dependent on glycolysis to maintain energy production. A metabolic symbiosis has been suggested to exist between glycolytic and

*Abbreviations:* 3′ UTR, Three prime untranslated region; ATP6V0E1, ATPase $H^+$ transporting $V_0$ subunit e1; CDC42, cell division cycle 42; cDNA, DNA complementary to RNA; CWCS, Cumulative weighted context++ score; DEG, Differentially expressed gene; GO, Gene ontology; HCAR1, Hydroxycarboxylic acid receptor 1; KEGG, Kyoto Encyclopedia of Genes and Genomes; miRNA, microRNA; mRNA-Seq, mRNA sequencing; PARP1, poly(ADP-ribose) polymerase 1; PDAC, Pancreatic ductal adenocarcinoma; PI3K, Phosphoinositide 3-kinase; siRNA, Small interfering RNA; V-ATPase, Vacuolar ATPase.

* Corresponding author.
*E-mail address:* oyvind.haugen@stami.no (Ø.P. Haugen).
[1] Present address: STAMI – The National Institute of Occupational Health in Norway, P.O. Box 5330 Majorstuen, 0304 Oslo, Norway

https://doi.org/10.1016/j.gene.2022.146346
Received 24 July 2021; Received in revised form 16 January 2022; Accepted 15 February 2022
Available online 17 February 2022

oxidative cancer cells (Sonveaux et al., 2008). Lactate, the end product of glycolysis, is released by the hypoxic cells and taken up by cells in the tumour periphery, where it can fuel oxidative metabolism (Sonveaux et al., 2008; Kennedy et al., 2013). As a consequence, glucose is spared and can diffuse into the hypoxic regions to fuel glycolysis. Such a symbiotic relationship has also been reported in PDAC tumours (Guillaumond et al., 2013). A heterogeneous distribution of monocarboxylate transporters (MCTs) enables passive transport of lactate between tumour compartments (Pérez-Escuredo et al., 2016).

In 2014, Roland and colleagues discovered the expression of hydroxycarboxylic acid receptor 1 (HCAR1) in a variety of cancer cell lines (Roland et al., 2014). This G protein-coupled receptor (GPCR), whose endogenous ligand is lactate, was upregulated in 148 of 158 resected PDAC tumours. The authors found that HCAR1 regulated MCT expression and was crucial for PDAC cell survival when lactate was the only available energy source. This indicates that HCAR1 has a prominent role in regulating lactate exchange between PDAC cells. In addition, HCAR1 expression correlated with PDAC tumour growth and metastasis *in vivo* (Roland et al., 2014).

It was recently shown that lactate increased the transcriptional activity of *HCAR1* through binding of signal transducer and activator of transcription 3 (STAT3) to the *HCAR1* promoter in lung cancer cell lines (Xie et al., 2020). Apart from this, little is known about the regulation of *HCAR1*. It is estimated that >60% of human protein-coding genes are conserved targets of microRNA (miRNA) regulation (Friedman et al., 2009). miRNAs are small endogenous RNAs that regulate gene expression through post-transcriptional repression (Bartel, 2018). Aberrant miRNA expression is frequently found in cancers (Rupaimoole and Slack, 2017), potentially affecting the expression of hundreds of direct target genes (Friedman et al., 2009). miRNAs therefore have potential as diagnostic and prognostic biomarkers and are being explored as therapeutic targets or tools (Rupaimoole and Slack, 2017).

The aim of this study was to investigate the potential miRNA-mediated regulation of HCAR1. We identified miR-431-5p as a possible regulator and confirmed its interaction with the 3′ UTR of HCAR1. Functional experiments in combination with transcriptomic analyses were used to further investigate the function of this miRNA in PDAC cells.

## 2. Results

### 2.1. miR-431-5p is a predicted regulator of HCAR1 and directly targets the 3′ UTR

As no validated miRNA has been reported for *HCAR1*, we used TargetScanHuman to predict miRNAs that could target *HCAR1*. TargetScanHuman uses a prediction algorithm that considers the site type and the sum of 14 additional features, termed the cumulative weighted context++ score (CWCS), to predict target site efficacy (Agarwal et al., 2015). A more negative CWCS predicts stronger repression. Excluding poorly conserved miRNA families, which are less likely to exert a beneficial biological function than conserved miRNAs (Bartel, 2018), miR-431-5p had the most negative CWCS of the predicted miRNAs (see supplementary material). Two non-conserved 7mer-m8 target sites were predicted within the 3′ UTR of *HCAR1* (Fig. 1A). The 3′ UTR reporter assay showed direct binding of miR-431-5p to the 3′ UTR of *HCAR1*, as indicated by a significant decrease in luciferase activity (Fig. 1B). We therefore proceeded to study its function in PDAC cells.

### 2.2. Expression of miR-431-5p and HCAR1 shows a negative relationship in PDAC cell lines

The endogenous expression of miR-431-5p and HCAR1 was analyzed by RT-qPCR in the PDAC cell lines. No miR-431-5p expression was found in BxPC-3 and Capan-2 cells, whereas a notable expression was found in PANC-1 cells (Fig. 2A). The relative expression of miR-431-5p cannot be calculated as it was only detected in PANC-1 cells. We therefore present the quantitation cycle values (Cq values). The Cq value is obtained from where the fluorescent signal is above background and is inversely proportional to the number of target copies in the sample, i.e. the higher the expression, the lower the Cq value. Given a 100% efficient PCR reaction, one Cq value difference equals a two-fold difference in expression. A mean Cq value of 23.9 for miR-431-5p was observed in PANC-1 cells, indicating a much higher expression than in BxPC-3 and Capan-2 cells, where no Cq values were obtained (detection limit at Cq = 40). HCAR1 expression was present in all the cell lines, but was considerably higher in BxPC-3 and Capan-2 cells relative to PANC-1 cells (Fig. 2B).

### 2.3. miR-431-5p overexpression inhibits cell proliferation

Transfection with miR-431-5p mimic had a negative impact on cell proliferation in the PDAC cell lines, as confirmed by cell counting (Fig. 3A-C). The effect was most pronounced in the BxPC-3 cells, where

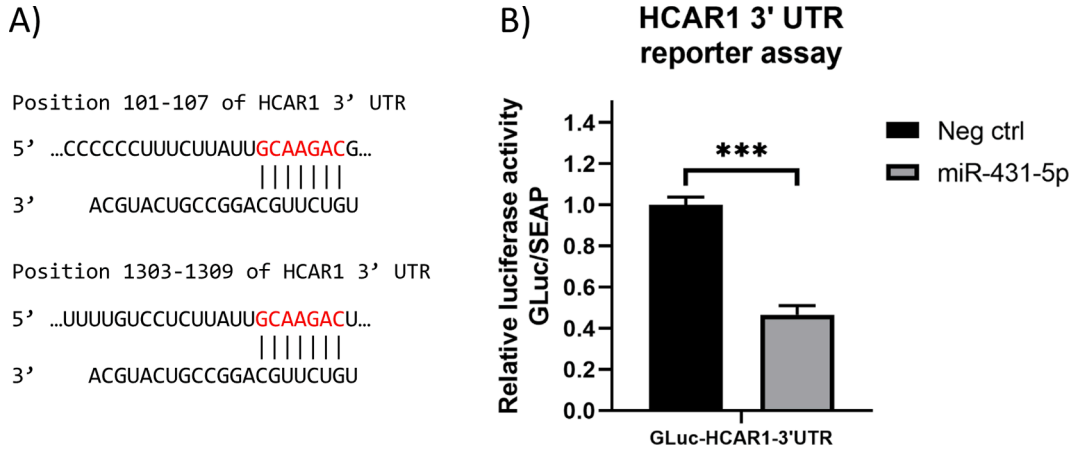


**Fig. 1. HCAR1 is a target of miR-431-5p. (A)** The two target sites of miR-431-5p within the 3′ UTR of *HCAR1* as predicted by TargetScanHuman. Both sites are 7mer-m8 types, meaning that there is an exact match to positions 2–8 of the miRNA. **(B)** 3′ UTR reporter assay confirmed the direct interaction of miR-431-5p and the 3′ UTR of *HCAR1*, indicated by the decreased luciferase activity in HEK-293T transfected with miR-431-5p mimic and HCAR1 3′ UTR reporter construct. The mean ± SD of three independent experiments is shown. Paired *t*-test, ***P < 0.001.

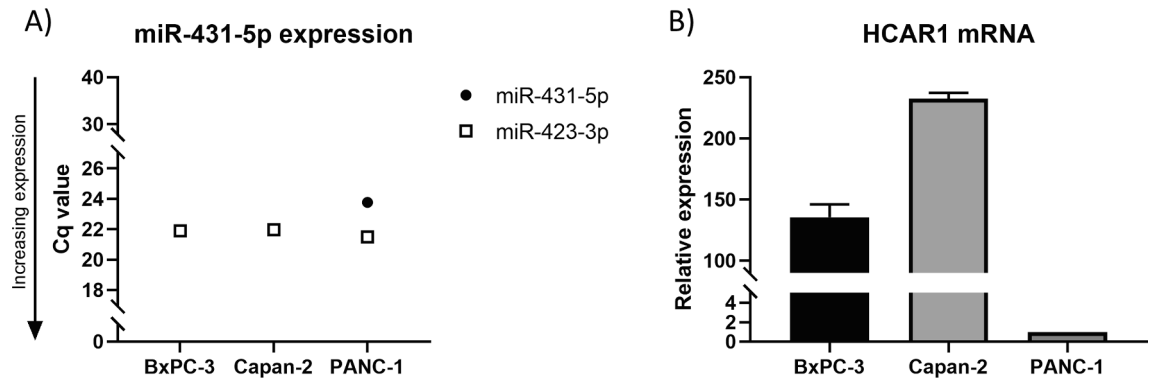


**Fig. 2. Endogenous expression of miR-431-5p and HCAR1 in three PDAC cell lines. (A)** Dot plot showing the Cq values for miR-431-5p expression in BxPC-3, Capan-2, and PANC-1 cells. The Cq value is obtained from where the fluorescent signal is above background and is inversely proportional to the number of target copies in the sample, i.e. the higher the expression, the lower the Cq value. Given a 100% efficient PCR reaction, one Cq value difference equals a two-fold difference in expression. miR-431-5p expression was not detected in BxPC-3 and Capan-2 cells, whereas PANC-1 cells showed notable expression with a mean Cq value of 23.9. miR-423-3p was used as a housekeeping gene to verify equal loading of cDNA. Standard deviations are too small to be visualized. **(B)** HCAR1 expression in the same cell lines. Relative expression is shown with PANC-1 set to 1. The mean ± SD of triplicates is shown. Cq, quantitative cycle.

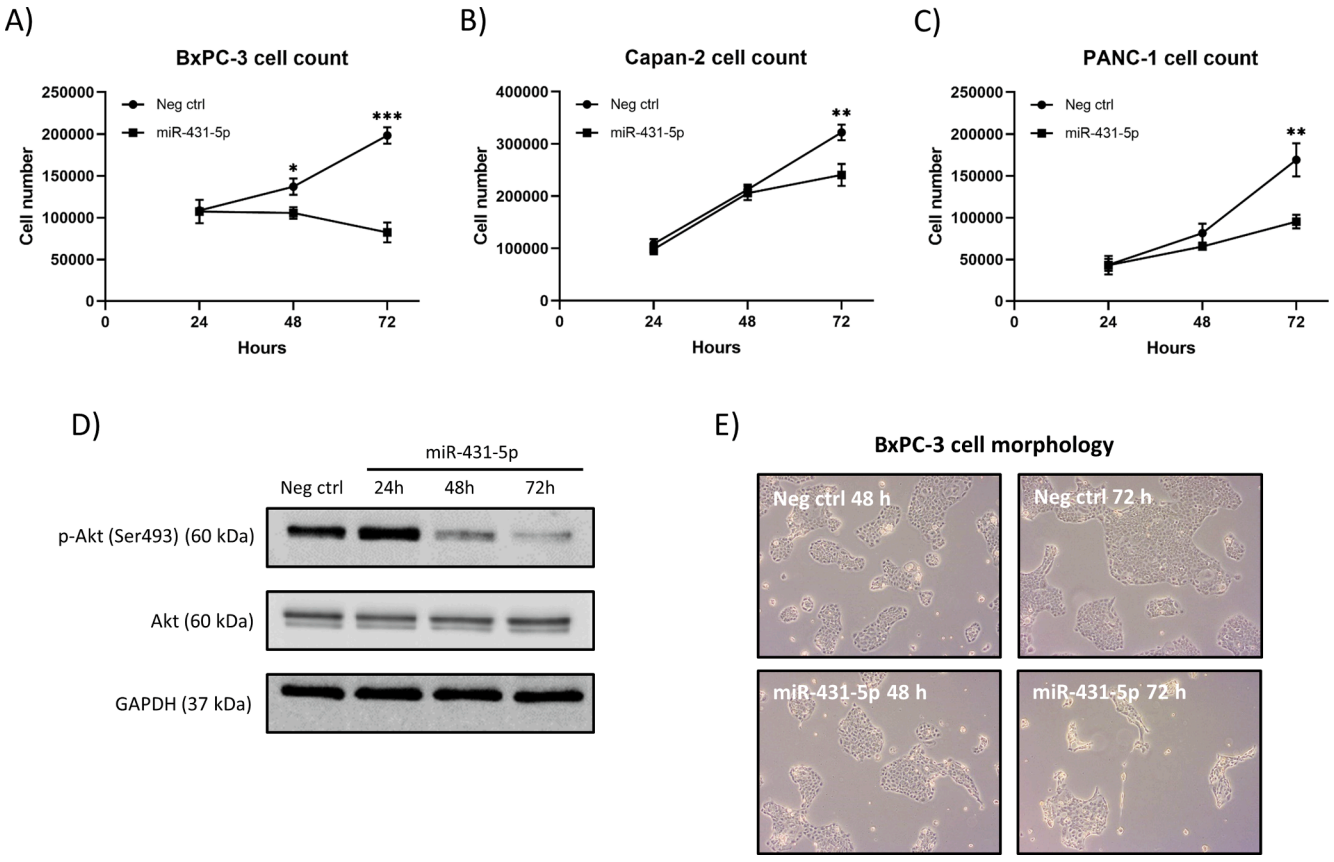


**Fig. 3. miR-431-5p overexpression inhibits cell proliferation. (A-C)** Transfection with miR-431-5p mimic inhibited proliferation of BxPC-3, Capan-2, and PANC-1 cells. The effect was most pronounced in BxPC-3 cells, with miR-431-3p overexpressing cells having stopped proliferating after 24 h and started to die after 48 h. The mean ± SD of three independent experiments is shown. Paired *t*-test, statistical significance *P < 0.05, **P < 0.01, ***P < 0.001. **(D)** Western blot showing reduced Akt phosphorylation 48 and 72 h post transfection with mimic. Control is lysate from cells transfected with negative control siRNA for 72 h. **(E)** Light microscopy of BxPC-3 cells showing a change in morphology from 48 to 72 h after transfection with mimic.

overexpression inhibited cell growth completely, and a significant difference in cell number compared to control was found 48 and 72 h after transfection. After 72 h, the cell number had declined and become approximately 40% of the number of control cells. In accordance with the cell counts, western blotting showed decreased Akt phosphorylation (p-Akt) after 48 and 72 h (Fig. 3D). Light microscopy showed a notable change in cell morphology to abnormally looking cells (Fig. 3E). Capan-2 and PANC-1 cells overexpressing miR-431-5p showed continued growth, although at a slower rate compared to their respective controls, with a significant difference found 72 h after transfection.

### 2.4. *mRNA-Seq reveals thousands of DEGs*

Sequencing the transcriptome of miR-431-5p overexpressing BxPC-3

cells revealed hundreds of uniquely expressed genes, meaning that these genes had been turned on or off when compared to their initial expression state (Fig. 4A). In addition, we found thousands of DEGs: 3679 after 24 h, 4556 after 48 h, and 4639 after 72 h (Fig. 4B). Volcano plots (Fig. 4C-E) show a near symmetrical distribution of the number of DEGs that were up- or downregulated. After scaling the relative abundance of DEGs on a per-gene basis, we clustered the DEGs and samples based on similar expression patterns. The generated heatmap shows the hierarchical relationship between the samples based on their DEG profiles (Fig. 4F). The DEG profiles of miR-431-5p transfected cells after 48 h and 72 h were more similar to each other than to the profile after 24 h.

### 2.5. Functional annotation of DEGs

Biological information from the large set of DEGs was retrieved and interpreted using GO term and KEGG pathway enrichment analyses. The complete lists of significantly enriched GO terms and KEGG pathways can be found in the supplementary material.

GO term enrichment analysis annotates genes to predefined GO terms that describe their function. All terms are associated with one of three main ontologies: Biological process, Cellular component, and Molecular function. Here, we show the top 30 significantly enriched GO terms associated with "Biological process", whose terms describe the larger biological processes of the annotated genes (Table 1). miR-431-5p transfected cells showed enrichment of six cell death-related GO terms after 24 h (cell death, programmed cell death, regulation of cell death, regulation of programmed cell death, apoptotic process, regulation of apoptotic process), indicating that the onset of apoptosis occurred shortly after transfection. While these remained among the significantly enriched GO terms after 48 h and 72 h, they were no longer among the top 30 since other GO terms became more enriched. After 48 h, the 10 most enriched GO terms could be linked to cell cycle and cell division processes (mitotic cell cycle, mitotic cell cycle process, mitotic nuclear division, cell division, organelle fission, nuclear division, cell cycle process, cell cycle, chromosome organization). After 72 h, 21 of the 30 most significantly enriched GO terms were the same as that after 48 h, indicating that the effects of miR-431-5p transfection had stabilized.

For the KEGG pathway enrichment analysis, we focused on those related to Pathways in cancer (KEGG Pathway: hsa05200) (Table 2). Of these, the following were significantly enriched during all time points: PPAR signaling pathway, MAPK signaling pathway, cAMP signaling pathway, Cytokine–cytokine receptor interaction, HIF-1 signaling pathway, Cell cycle, p53 signaling pathway, mTOR signaling pathway, PI3K–Akt signaling pathway, Apoptosis, Wnt signaling pathway, Notch signaling pathway, TGF-beta signaling pathway, VEGF signaling pathway, Focal adhesion, ECM-receptor interaction, Adherens junction, JAK–STAT signaling pathway, and Estrogen signaling pathway. The Hedgehog signaling pathway was significantly enriched after 24 h and 48 h, but not after 72 h.

### 2.6. miR-431-5p overexpression disrupts cell cycle progression and induces apoptosis

The cell counts and sequencing data encouraged us to study possible changes in cell cycle progression and activation of apoptosis in BxPC-3 cells. miR-431-5p overexpression led to a significant shift in cell cycle distribution, with an increased number of cells in the G1/G0 phase and a reduced number of cells in S phase (Fig. 5B). Western blotting showed

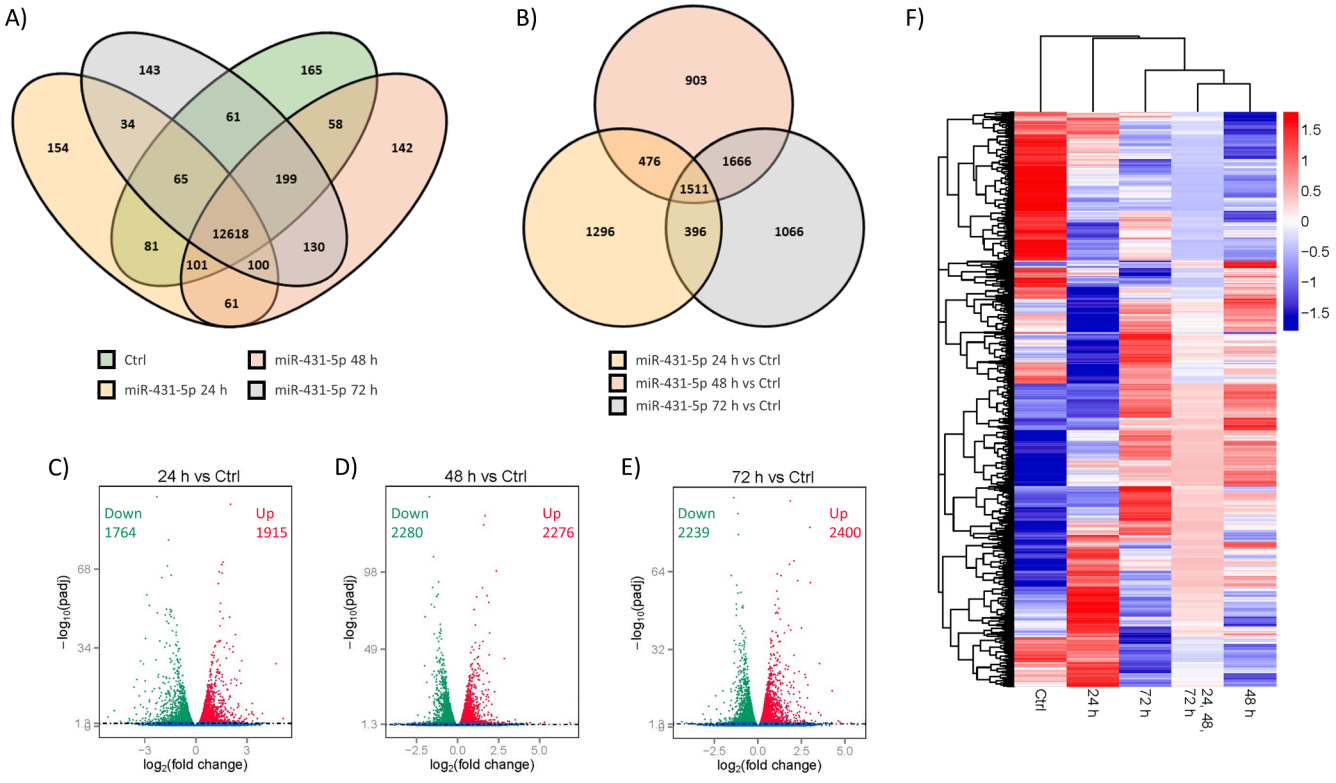


**Fig. 4. Graphical presentation of differentially expressed genes.** BxPC-3 cells were transfected with miR-431-5p mimic, and mRNA was isolated after 24 h, 48 h, and 72 h. Cells transfected with negative control siRNA for 72 h were used as control. The data presented is the mean of three independent experiments. **(A)** Venn diagram showing the number of genes that are uniquely expressed or shared between samples (FPKM $\geq$ 1). **(B)** Venn diagram showing the number of DEGs within each sample ($P_{adj} < 0.05$), with intersections showing the number of DEGs shared between samples. **(C-E)** Volcano plots showing down- (green) and up-regulated (red) DEGs for each sample. The x-axis shows the $\log_2$ fold change in gene expression, and the y-axis shows the level of statistical difference. **(F)** Cluster analysis of DEGs, where genes (rows) and samples (columns) have been clustered based on similar expression patterns. Each row of the heatmap represents the z-score transformed $\log_{10}$(FPKM + 1) values of one DEG across all samples (blue: low expression, red: high expression). DEG, differentially expressed gene. (For interpretation of the references to colour in this figure legend, the reader is referred to the web version of this article.)

**Table 1**

**Enriched GO terms.** Top 30 significantly enriched GO terms associated with the main ontology «Biological process» at the different time points in BxPC-3 cells transfected with miR-431-5p mimic. Enrichment was calculated by dividing the number of DEGs (input) on the total number of genes assigned to the pathway (background). Statistical significance $P_{adj} < 0.05$. GO, Gene Ontology; DEG, differentially expressed gene.

| 24 hours | | | | | 48 hours | | | | | 72 hours | | | | |
|---|---|---|---|---|---|---|---|---|---|---|---|---|---|---|
| GO accession | Description | Input/background | Enrichment | Adj. P value | GO accession | Description | Input/background | Enrichment | Adj. P value | GO accession | Description | Input/background | Enrichment | Adj. P value |
| GO:0006950 | response to stress | 934/3824 | 0,24 | 2,39E-25 | GO:0071840 | cellular component organization or biogenesis | 1781/5925 | 0,30 | 1,04E-49 | GO:0071840 | cellular component organization or biogenesis | 1729/5925 | 0,29 | 1,44E-34 |
| GO:0048519 | negative regulation of biological process | 1050/4366 | 0,24 | 5,56E-24 | GO:0016043 | cellular component organization | 1746/5804 | 0,30 | 2,62E-48 | GO:0016043 | cellular component organization | 1696/5804 | 0,29 | 7,13E-34 |
| GO:0048523 | negative regulation of cellular process | 975/4040 | 0,24 | 4,13E-22 | GO:0006996 | organelle organization | 1138/3469 | 0,33 | 1,77E-46 | GO:0008152 | metabolic process | 3025/11549 | 0,26 | 4,56E-31 |
| GO:0048518 | positive regulation of biological process | 1213/5207 | 0,23 | 6,79E-22 | GO:0007049 | cell cycle | 622/1674 | 0,37 | 3,66E-39 | GO:0071704 | organic substance metabolic process | 2718/10301 | 0,26 | 7,94E-27 |
| GO:0048583 | regulation of response to stimulus | 858/3473 | 0,25 | 8,35E-22 | GO:0000278 | mitotic cell cycle | 413/1005 | 0,41 | 9,68E-37 | GO:0006996 | organelle organization | 1063/3469 | 0,31 | 1,30E-26 |
| GO:0010033 | response to organic substance | 701/2743 | 0,26 | 6,09E-21 | GO:0044267 | cellular protein metabolic process | 1402/4745 | 0,30 | 2,82E-32 | GO:0044710 | single-organism metabolic process | 1486/5164 | 0,29 | 1,30E-26 |
| GO:0009966 | regulation of signal transduction | 649/2498 | 0,26 | 3,27E-20 | GO:0022402 | cell cycle process | 480/1260 | 0,38 | 3,49E-32 | GO:0044237 | cellular metabolic process | 2613/9867 | 0,26 | 3,97E-26 |
| GO:0048522 | positive regulation of cellular process | 1051/4463 | 0,24 | 1,21E-19 | GO:1902589 | single-organism organelle organization | 814/2462 | 0,33 | 1,56E-31 | GO:0044267 | cellular protein metabolic process | 1378/4745 | 0,29 | 3,82E-25 |
| GO:0008219 | cell death | 519/1938 | 0,27 | 1,98E-19 | GO:1903047 | mitotic cell cycle process | 349/839 | 0,42 | 1,77E-31 | GO:0044238 | primary metabolic process | 2629/9968 | 0,26 | 9,01E-25 |
| GO:0070887 | cellular response to chemical stimulus | 654/2564 | 0,26 | 2,62E-19 | GO:0008152 | metabolic process | 2987/11547 | 0,26 | 5,58E-30 | GO:0033554 | cellular response to stress | 613/1831 | 0,33 | 3,45E-23 |
| GO:0051128 | regulation of cellular component organization | 544/2043 | 0,27 | 3,03E-19 | GO:0019538 | protein metabolic process | 1535/5349 | 0,29 | 2,61E-29 | GO:0019538 | protein metabolic process | 1512/5349 | 0,28 | 1,21E-22 |
| GO:0032268 | regulation of cellular protein metabolic process | 598/2322 | 0,26 | 7,55E-19 | GO:0044237 | cellular metabolic process | 2599/9867 | 0,26 | 2,15E-28 | GO:0007049 | cell cycle | 565/1674 | 0,34 | 1,02E-21 |
| GO:0012501 | programmed cell death | 494/1842 | 0,27 | 1,69E-18 | GO:0043933 | macromolecular complex subunit organization | 778/2436 | 0,32 | 4,34E-27 | GO:0033036 | macromolecule localization | 846/2736 | 0,31 | 1,75E-21 |
| GO:0051246 | regulation of protein metabolic process | 631/2488 | 0,25 | 2,08E-18 | GO:0033554 | cellular response to stress | 622/1831 | 0,34 | 7,66E-27 | GO:0006464 | cellular protein modification process | 1088/3651 | 0,30 | 1,59E-20 |
| GO:0006915 | apoptotic process | 488/1821 | 0,27 | 3,10E-18 | GO:0007067 | mitotic nuclear division | 195/403 | 0,48 | 9,38E-27 | GO:0036211 | protein modification process | 1088/3651 | 0,30 | 1,59E-20 |
| GO:0023051 | regulation of signaling | 711/2837 | 0,25 | 3,84E-18 | GO:0044260 | cellular macromolecule metabolic process | 2197/8144 | 0,27 | 3,39E-26 | GO:0008104 | protein localization | 748/2392 | 0,31 | 3,08E-20 |
| GO:0010646 | regulation of cell communication | 718/2879 | 0,25 | 8,61E-18 | GO:0071704 | organic substance metabolic process | 2682/10301 | 0,26 | 1,10E-25 | GO:0043412 | macromolecule modification | 1123/3809 | 0,29 | 6,23E-20 |
| GO:0002376 | immune system process | 618/2490 | 0,25 | 1,34E-17 | GO:0044238 | primary metabolic process | 2604/9968 | 0,26 | 2,95E-25 | GO:0000278 | mitotic cell cycle | 366/1005 | 0,36 | 7,26E-20 |
| GO:0035556 | intracellular signal transduction | 658/2628 | 0,25 | 3,34E-17 | GO:0043170 | macromolecule metabolic process | 2336/8805 | 0,27 | 5,56E-24 | GO:0044699 | single-organism process | 3344/13346 | 0,25 | 1,66E-19 |
| GO:0048584 | positive regulation of response to stimulus | 493/1886 | 0,26 | 1,57E-16 | GO:0051276 | chromosome organization | 375/1013 | 0,37 | 1,68E-23 | GO:0008150 | biological_process | 3996/16507 | 0,24 | 2,77E-19 |
| GO:0033554 | cellular response to stress | 482/1831 | 0,26 | 1,74E-16 | GO:0044710 | single-organism metabolic process | 1451/5164 | 0,28 | 2,96E-23 | GO:0006950 | response to stress | 1104/3824 | 0,29 | 2,90E-19 |
| GO:0031399 | regulation of protein modification process | 439/1625 | 0,27 | 1,90E-16 | GO:0051301 | cell division | 265/644 | 0,41 | 1,05E-22 | GO:0009987 | cellular process | 3663/14844 | 0,25 | 6,91E-19 |
| GO:0065009 | regulation of molecular function | 661/2670 | 0,25 | 2,14E-16 | GO:0009987 | cellular process | 3641/14844 | 0,25 | 2,72E-22 | GO:1903047 | mitotic cell cycle process | 311/839 | 0,37 | 1,19E-17 |
| GO:0032269 | negative regulation of cellular protein metabolic process | 286/971 | 0,29 | 2,56E-16 | GO:0006464 | cellular protein modification process | 1083/3651 | 0,30 | 1,68E-21 | GO:0044763 | single-organism cellular process | 3054/12075 | 0,25 | 1,36E-17 |
| GO:0042981 | regulation of apoptotic process | 386/1404 | 0,27 | 4,74E-16 | GO:0036211 | protein modification process | 1083/3651 | 0,30 | 1,68E-21 | GO:0044260 | cellular macromolecule metabolic process | 2161/8144 | 0,27 | 1,54E-17 |
| GO:0043067 | regulation of programmed cell death | 389/1417 | 0,27 | 4,75E-16 | GO:0044699 | single-organism process | 3318/13346 | 0,25 | 3,07E-21 | GO:1902589 | single-organism organelle organization | 756/2462 | 0,31 | 1,94E-17 |
| GO:0010941 | regulation of cell death | 406/1497 | 0,27 | 6,11E-16 | GO:0043412 | macromolecule modification | 1118/3809 | 0,29 | 5,92E-21 | GO:0048523 | negative regulation of cellular process | 1159/4040 | 0,29 | 6,89E-17 |
| GO:0044699 | single-organism process | 2648/13346 | 0,20 | 7,03E-16 | GO:0048285 | organelle fission | 231/554 | 0,42 | 8,12E-21 | GO:0051641 | cellular localization | 870/2931 | 0,30 | 1,44E-16 |
| GO:0016477 | cell migration | 331/1150 | 0,29 | 8,31E-16 | GO:0000280 | nuclear division | 218/520 | 0,42 | 6,28E-20 | GO:0034613 | cellular protein localization | 499/1542 | 0,32 | 3,05E-16 |
| GO:0010647 | positive regulation of cell communication | 405/1497 | 0,27 | 1,58E-15 | GO:0044763 | single-organism cellular process | 3033/12075 | 0,25 | 2,32E-19 | GO:0070727 | cellular macromolecule localization | 501/1550 | 0,32 | 3,34E-16 |

**Table 2**

**KEGG analysis of enriched pathways in cancer.** Enriched KEGG pathways related to Pathways in cancer (KEGG Pathway: hsa05200) at the different time points in BxPC-3 cells overexpressing miR-431-5p. Enrichment was calculated by dividing the number of DEGs (input) on the total number of genes assigned to the pathway (background). Statistical significance $P_{adj} < 0.05$. KEGG, Kyoto Encyclopedia of Genes and Genomes; DEG, differentially expressed gene.

| | 24 hours | | | 48 hours | | | 72 hours | | |
|---|---|---|---|---|---|---|---|---|---|
| Pathways in cancer | Input/background | Enrichment | Adj. P value | Input/background | Enrichment | Adj. P value | Input/background | Enrichment | Adj. P value |
| Adherens junction | 22/74 | 0,30 | 3,80E-05 | 31/74 | 0,42 | 2,37E-07 | 30/74 | 0,41 | 7,54E-07 |
| Hedgehog signaling pathway | 12/42 | 0,29 | 5,51E-03 | 11/42 | 0,26 | 4,39E-02 | 10/42 | 0,24 | 8,05E-02 |
| Notch signaling pathway | 10/48 | 0,21 | 2,98E-02 | 17/48 | 0,35 | 5,17E-04 | 20/48 | 0,42 | 3,59E-05 |
| HIF-1 signaling pathway | 32/103 | 0,31 | 3,65E-07 | 35/103 | 0,34 | 1,57E-06 | 42/103 | 0,41 | 4,32E-09 |
| Apoptosis | 47/140 | 0,34 | 7,66E-11 | 44/140 | 0,31 | 3,84E-07 | 43/140 | 0,31 | 1,05E-06 |
| TGF-B signaling pathway | 23/84 | 0,27 | 6,57E-05 | 24/84 | 0,29 | 4,78E-04 | 27/84 | 0,32 | 5,32E-05 |
| Wnt signaling pathway | 29/143 | 0,20 | 4,94E-04 | 34/143 | 0,24 | 5,17E-04 | 44/143 | 0,31 | 7,78E-07 |
| VEGF signaling pathway | 14/61 | 0,23 | 5,87E-03 | 22/61 | 0,36 | 6,26E-05 | 26/61 | 0,43 | 1,92E-06 |
| p53 signaling pathway | 26/69 | 0,38 | 3,02E-07 | 29/69 | 0,42 | 5,56E-07 | 28/69 | 0,41 | 1,57E-06 |
| ECM-receptor interaction | 25/82 | 0,30 | 8,30E-06 | 26/82 | 0,32 | 7,14E-05 | 21/82 | 0,26 | 2,93E-03 |
| Focal adhesion | 61/203 | 0,30 | 5,74E-12 | 71/203 | 0,35 | 2,94E-12 | 78/203 | 0,38 | 7,10E-15 |
| cAMP signaling pathway | 42/199 | 0,21 | 1,61E-05 | 40/199 | 0,20 | 2,31E-03 | 48/199 | 0,24 | 3,92E-05 |
| mTOR signaling pathway | 41/154 | 0,27 | 2,19E-07 | 53/154 | 0,34 | 2,86E-09 | 58/154 | 0,38 | 5,24E-11 |
| Cell cycle | 40/124 | 0,32 | 4,51E-09 | 65/124 | 0,52 | 2,29E-17 | 57/124 | 0,46 | 1,39E-13 |
| PI3K-Akt signaling pathway | 82/342 | 0,24 | 1,45E-11 | 89/342 | 0,26 | 1,35E-09 | 103/342 | 0,30 | 7,64E-14 |
| Cytokine-cytokine receptor interaction | 60/265 | 0,23 | 3,47E-08 | 43/265 | 0,16 | 2,98E-02 | 52/265 | 0,20 | 1,03E-03 |
| Jak-STAT signaling pathway | 36/158 | 0,23 | 1,75E-05 | 28/158 | 0,18 | 3,30E-02 | 33/158 | 0,21 | 3,50E-03 |
| MAPK signaling pathway | 66/255 | 0,26 | 9,01E-11 | 61/255 | 0,24 | 3,57E-06 | 70/255 | 0,27 | 2,12E-08 |
| Estrogen signaling pathway | 24/99 | 0,24 | 1,96E-04 | 24/99 | 0,24 | 2,70E-03 | 28/99 | 0,28 | 2,04E-04 |
| Calcium signaling pathway | 24/180 | 0,13 | 7,09E-02 | 29/180 | 0,16 | 7,01E-02 | 29/180 | 0,16 | 7,49E-02 |
| PPAR signaling pathway | 16/72 | 0,22 | 4,47E-03 | 19/72 | 0,26 | 3,44E-03 | 21/72 | 0,29 | 8,78E-04 |

decreased levels of CDC42 protein, which normally functions in G1 to S phase progression (Fig. 5C) (Olson et al., 1995). Phosphatidylserine labeling on the outer surface of the plasma membrane showed a stronger signal in cells overexpressing miR-431-5p, indicating ongoing apoptosis (Fig. 5E). Supporting this, western blotting showed decreased levels of survivin (inhibitor of apoptosis) and the appearance of the 24 kDa apoptotic fragment of cleaved PARP1 (Fig. 5F). Fig. 5A and D show the ancestor charts showing the parental structure of the enriched GO terms related to cell cycle and apoptosis, respectively.

### 2.7. *HCAR1 knockdown does not affect cell viability*

siRNA-mediated knockdown of *HCAR1* in BxPC-3 cells reduced mRNA expression by approximately 65% (Fig. 6A). Cell counts showed that cell proliferation remained unchanged when compared to the control cells (Fig. 6B).

### 2.8. *V-ATPase Subunit e is a target of miR-431-5p*

As knockdown of *HCAR1* did not affect cell viability, we looked for other candidate targets of miR-431-5p that could contribute to the effects of miR-431-5p overexpression. TargetScanHuman showed that *ATP6V0E1* was among the top of the 169 predicted targets with conserved sites for miR-431-5p, containing one conserved 8mer target site within its 3′ UTR (Fig. 7A). *ATP6V0E1* encodes the membrane-bound subunit e of V-ATPase, which influences many cancer-associated processes, including cell growth and apoptosis (Stransky et al., 2016). Our mRNA-Seq data showed that *ATP6V0E1* was the second most repressed DEG across all time points when sorting on adjusted P-value. For the complete lists of DEGs, see the supplementary material. Direct interaction of miR-431-5p to the 3′ UTR of *ATP6V0E1* was confirmed by 3′ UTR reporter assay (Fig. 7B).

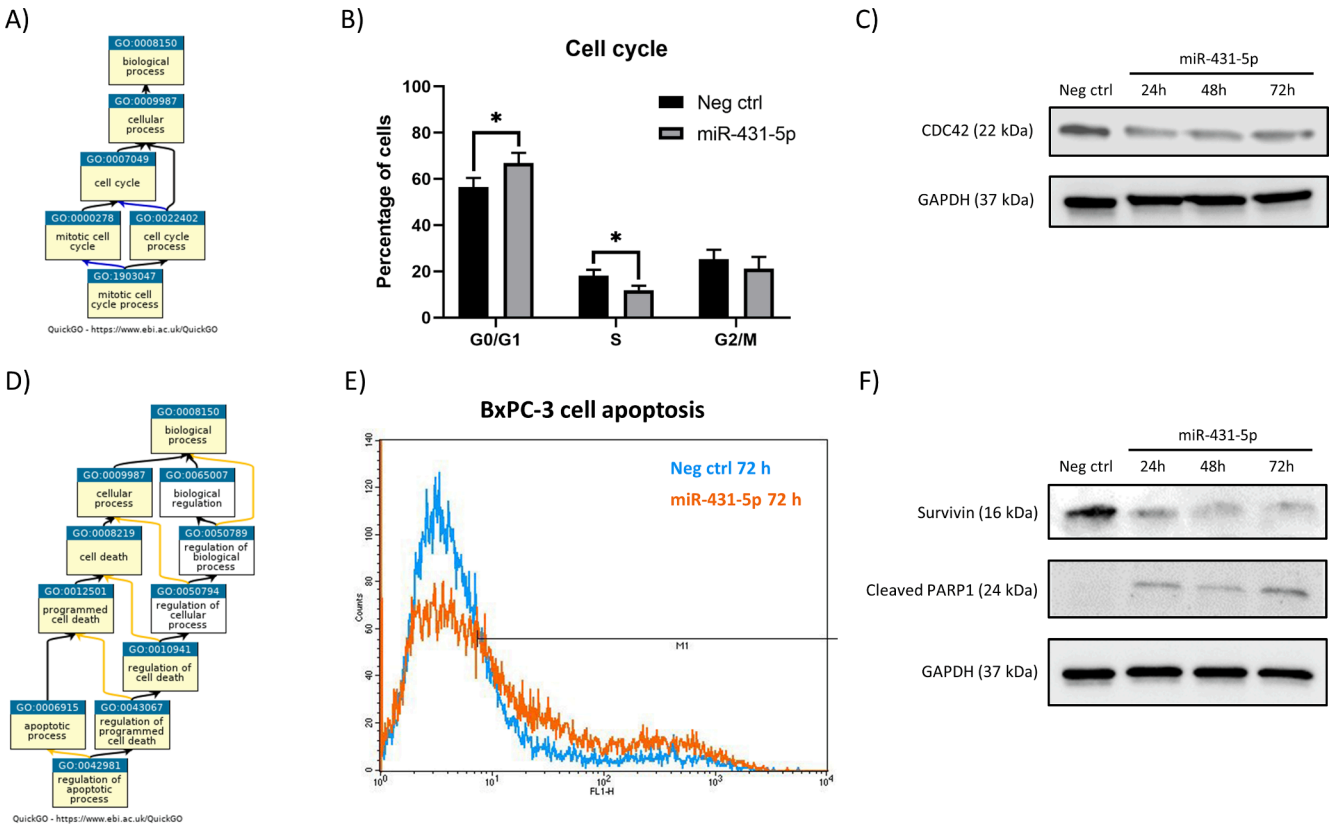


**Fig. 5. miR-431-5p overexpression disrupts cell cycle progression and induces apoptosis. (A)** Ancestor chart showing the parental structure of GO terms related to the cell cycle from the top 30 significantly enriched GO terms (yellow boxes) 48 h after transfection with miR-431-5p mimic. Arrow colour describes the relationship between parental and child terms, where black arrow means «is a» and blue arrow means «part of». **(B)** The percentage of cells distributed over the different cell cycle phases. Overexpression of miR-431-5p increased the percentage of cells in the G1/G0 phase and reduced the percentage of cells in the S phase. The mean ± SD of three independent experiments is shown. Paired *t*-test, *P < 0.05. **(C)** Western blot showed decreased CDC42 in miR-431-5p overexpressing cells compared to control (negative control siRNA 72 h). **(D)** Ancestor chart showing the parental structure of GO terms related to apoptosis from the top 30 significantly enriched GO terms (yellow boxes) 24 h after transfection with miR-431-5p mimic. Arrow colour describes the relationship between parental and child terms, where black arrow means «is a» and yellow arrow means «regulates». **(E)** Flow cytometric analysis of live and apoptotic cells. The proportion of apoptotic cells was calculated by dividing the area under the set M1 line on the total graph area for each treatment group. The normalized proportions were then compared, and cells overexpressing miR-431-5p had a 61.4% increase in apoptosis compared to control cells 72 h after transfection. Graph areas were measured in ImageJ software. **(F)** Western blot showing decreased levels of survivin in miR-431-5p overexpressing cells compared to control (negative control siRNA 72 h) and appearance of a 24 kDa cleaved PARP1 fragment. (For interpretation of the references to colour in this figure legend, the reader is referred to the web version of this article.)

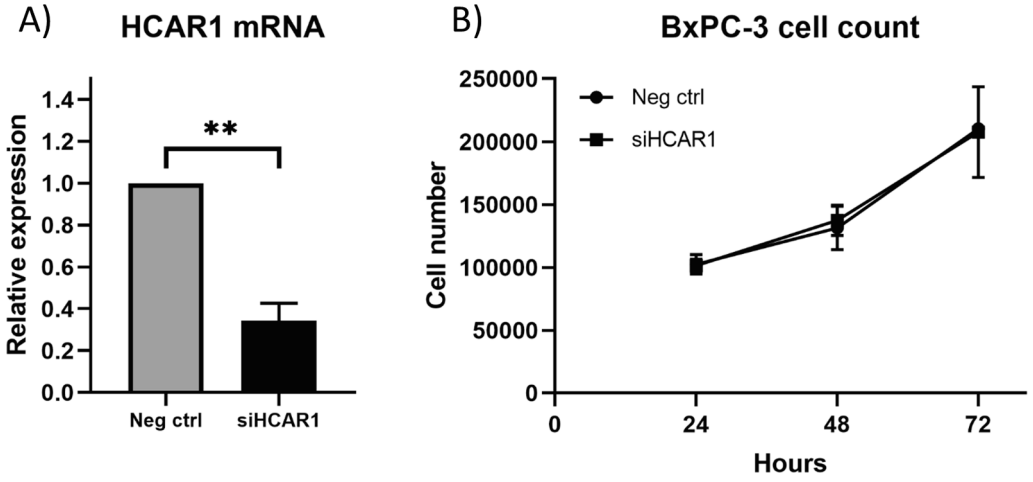


**Fig. 6. Knockdown of HCAR1 does not affect cell viability. (A)** siRNA-mediated knockdown of *HCAR1* in BxPC-3 cells resulted in a ~ 65% reduction in mRNA expression. **(B)** Knockdown of *HCAR1* did not affect the proliferation of BxPC-3 cells. The mean ± SD of three independent experiments is shown. Paired *t*-test, **P < 0.01.

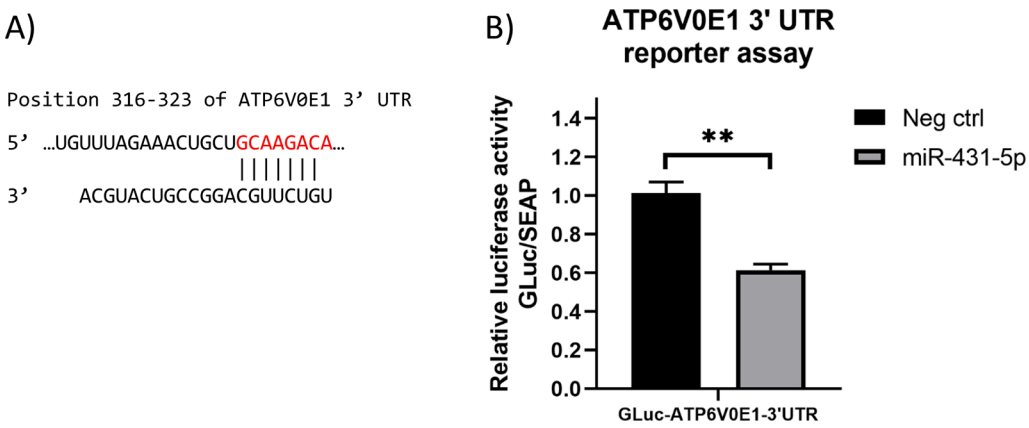


**Fig. 7. ATP6V0E1 is a target of miR-431-5p. (A)** The target site of miR-431-5p within the 3′ UTR of *ATP6V0E1* as predicted by TargetScanHuman. In addition to an exact match at positions 2–8 of the miRNA, the preference for adenine across the first nucleotide of the miRNA, despite no base pairing due to structural hindrance, defines an 8mer (Agarwal et al., 2015). **(B)** 3′ UTR reporter assay confirmed the direct interaction of miR-431-5p and the 3′ UTR of *ATP6V0E1*, indicated by the decreased luciferase activity in HEK-293 T transfected with miR-431-5p mimic and ATP6V0E1 3′ UTR reporter construct. The mean ± SD of three independent experiments is shown. Paired *t*-test, **P < 0.01.

### 2.9. Knockdown of ATP6V0E1 mimics the effect of miR-431-5p overexpression

siRNA-mediated knockdown of *ATP6V0E1* in BxPC-3 cells reduced mRNA expression by approximately 90% (Fig. 8A) and mimicked the effect of miR-431-5p overexpression in reducing cell viability (Fig. 8B) and inducing apoptosis (Fig. 8C). However, there were some noticeable differences. The reduction in cell numbers after 48 h was greater after *ATP6V0E1* knockdown than after miR-431-5p overexpression. In addition, cell cultures transfected with *ATP6V0E1* siRNA contained many individual scattered cells and smaller cell clusters (Fig. 8D) than the cultures transfected with miR-431-5p mimic (Fig. 3E).

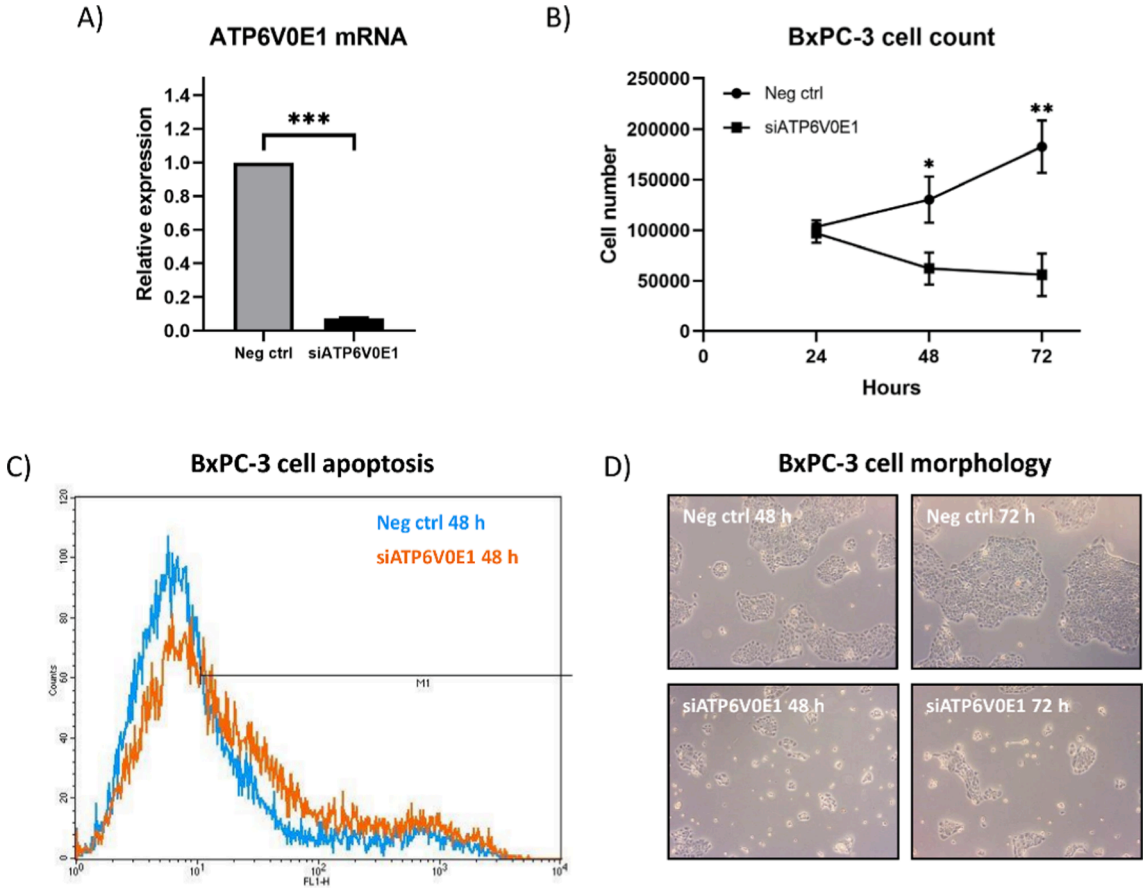


**Fig. 8. Knockdown of ATP6V0E1 mimics the effect of miR-431-5p overexpression. (A)** siRNA-mediated knockdown of *ATP6V0E1* in BxPC-3 cells resulted in a ~90% reduction in mRNA expression. The mean ± SD of three independent experiments is shown. Paired *t*-test, ***P < 0.001. **(B)** Knockdown of *ATP6V0E1* inhibited proliferation of BxPC-3 cells, and reduced cell numbers were observed after 48 and 72 h. The mean ± SD of three independent experiments is shown. Paired *t*-test, *P < 0.05, **P < 0.01. **(C)** Flow cytometric analysis of live and apoptotic cells. The proportion of apoptotic cells was calculated by dividing the area under the set M1 line on the total graph area for each treatment group. The normalized proportions were then compared, and siATP6V0E1-transfected BxPC-3 cells had a 60.6% increase in apoptosis compared to control cells 48 h after transfection. Graph areas were measured in ImageJ software. **(D)** Cultures with siATP6V0E1-transfected BxPC-3 cells showed many individually scattered cells and formation of small cell clusters.

### 2.10. RT-qPCR validation of HCAR1 and ATP6V0E1 repression

To validate the *HCAR1* and *ATP6V0E1* expression levels as measured by mRNA-Seq, we performed RT-qPCR on the same RNA samples that had been used for sequencing. The expression levels correlated well with the sequencing data and thus confirmed *HCAR1* and *ATP6V0E1* repression in the miR-431-5p overexpressing cells (Fig. 9A,B). Overexpression of miR-431-5p repressed *ATP6V0E1* expression by approximately 60–70% compared to the approximately 50% repression of *HCAR1*. This can be explained by the different target site types and their interaction efficacies, as predicted by TargetScanHuman (Agarwal et al., 2015). *ATP6V0E1* has one conserved 8mer site and a CWCS of −0.61 compared to the two non-conserved 7mer-m8 sites in *HCAR1* - with a CWCS of −0.40. Conserved sites are generally more effective than non-conserved sites because they tend to reside in locations with more favorable site contexts (Grimson et al., 2007).

## 3. Discussion

The lactate receptor HCAR1 is highly expressed in PDAC tumours, and its expression correlates with tumour growth and metastasis (Roland et al., 2014). We investigated whether *HCAR1* could be a target of miRNA regulation. We identified miR-431-5p as a predicted regulator and confirmed its direct interaction with the 3′ UTR of HCAR1. Endogenous miR-431-5p expression was absent in BxPC-3 and Capan-2 cells, while it was clearly present in PANC-1 cells. Conversely, BxPC-3 and Capan-2 showed the highest expression of *HCAR1*, while it was considerably lower in PANC-1 cells. This suggests a possible negative correlation between miR-431-5p and *HCAR1* expression, although a larger sample size would be required to confirm it.

Overexpressing miR-431-5p in PDAC cells inhibited proliferation, including PANC-1 cells which showed endogenous miR-431-5p expression. The most affected cell line, BxPC-3, showed reduced Akt phosphorylation after 48 and 72 h. The activity of the PI3K–Akt pathway, which has a prominent role in controlling cell proliferation and survival, is frequently elevated in cancer (Fruman et al., 2017). It is found to be overactive in primary PDAC cultures and cell lines, including BxPC-3 cells, by measuring p-Akt (Massihnia et al., 2017). The same study showed a negative correlation between p-Akt levels and survival. We found altered cell cycle progression and ongoing apoptosis in BxPC-3 cells overexpressing miR-431-5p, consistent with the reduced levels of p-Akt. The variation in response to miR-431-5p overexpression may reflect the heterogeneity of the cell lines. For example, phenotypic traits and mutations in key genetic drivers of PDAC progression (*KRAS*, *CDKN2A*, *TP53*, and *SMAD4*) vary considerably between commonly used PDAC cell lines, including those used in our study (Deer et al., 2010). In this context, it should be mentioned that while BxPC-3 cells contain wild-type *KRAS*, they also contain an in-frame deletion in *BRAF*, leading to a constitutively active KRAS effector pathway (Chen et al., 2016).

The results from our functional experiments were largely supported by the analysis of mRNA-Seq data from miR-431-5p overexpressing BxPC-3 cells, which in addition to *HCAR1*, revealed a large number of DEGs. The GO term enrichment analysis showed enrichment of GO terms describing processes of apoptosis and the cell cycle. The KEGG pathway enrichment analysis showed a substantial number of DEGs annotated to Pathways in cancer, and most of these signalling pathways have been extensively described with regards to PDAC progression (Bryant et al., 2014; Yuen and Díaz, 2014; Polireddy and Chen, 2016).

Our findings suggest that miR-431-5p functions as a tumour suppressor in PDAC cells. This is in agreement with a study showing that miR-431-5p overexpression induces apoptosis in PDAC cells (Yang et al., 2018), although it is unclear which PDAC cell line was used for overexpression. The same study showed reduced miR-431-5p expression in PDAC tissue and cell lines. Not much is known about the clinical relevance of miR-431-5p, but one study of miRNA expression in tissue samples from 225 patients diagnosed with pancreatic cancer (107 PDAC cases) revealed that miR-431-5p was a prognostic marker for overall survival, although only by one of two statistical methods (Schultz et al., 2012). In hepatocellular carcinoma (HCC) tissue samples, miR-431-5p expression was reduced and correlated with poor prognostic features (Sun et al., 2015). miR-431-5p inhibited epithelial–mesenchymal transition in HCC cells (Sun et al., 2015; Kong et al., 2018). Furthermore, miR-431-5p itself is downregulated by hsa_circ_0005075, a circulatory RNA found to be increased in HCC tissue and whose overexpression increases HCC cell proliferation, migration, and invasion (Li et al., 2018). Another study found miR-431-5p expression to be reduced in the lung carcinoids of patients with lymph node metastasis (Rapa et al., 2015).

siRNA-mediated knockdown of *HCAR1* did not affect cell viability. This was expected, as *HCAR1* silencing affects PDAC cells exclusively in culture conditions where lactate is the only available energy substrate (Roland et al., 2014). It is therefore unlikely that *HCAR1* repression alone contributes to the observed effects of miR-431-5p overexpression.

The predicted gene targets of miR-431-5p by TargetScanHuman, combined with our mRNA-Seq data, identified *ATP6V0E1* as a potential target. The direct interaction of miR-431-5p to the 3′ UTR of *ATP6V0E1* was confirmed. *ATP6V0E1* encodes subunit e of the membrane-bound domain ($V_0$) of V-ATPase, a proton pump that acidifies organelles along the endocytic pathway (Stransky et al., 2016). V-ATPase is often located in the plasma membrane of glycolytic cancer cells, where it maintains intracellular pH homeostasis and acidifies the tumour microenvironment by pumping out excess protons (Damaghi et al., 2013). Cancer cells are particularly sensitive to V-ATPase inhibition, which leads to the induction of apoptosis (Nakashima et al., 2003; Morimura et al., 2008; von Schwarzenberg et al., 2013). We therefore examined the effect of *ATP6V0E1* knockdown on BxPC-3 cells.

To a large extent, knockdown of *ATP6V0E1* mimicked the effect of

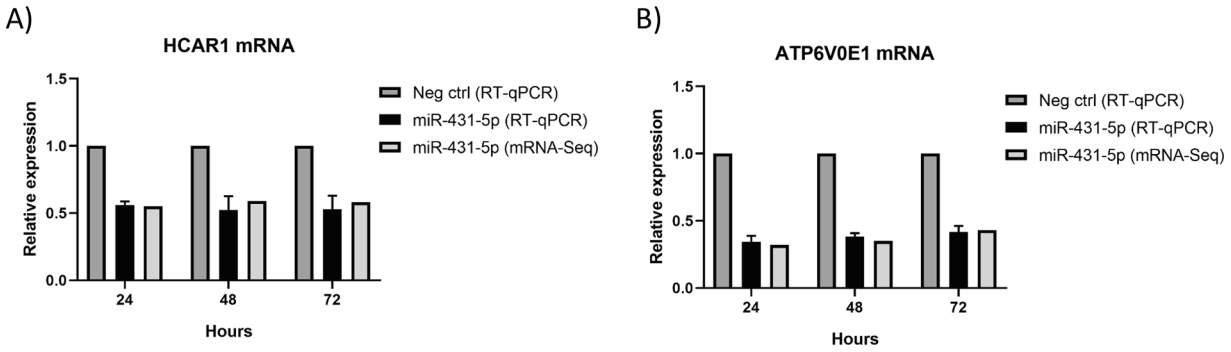


**Fig. 9. Validation of mRNA-Seq data for HCAR1 and ATP6V0E1 by RT-qPCR (A, B)** RT-qPCR validated the results from the mRNA-Seq on the same RNA samples, showing reduced *HCAR1* and *ATP6V0E1* mRNA levels after transfection with miR-431-5p mimic. The mean ± SD of three independent experiments is shown with the negative control set to 1.

miR-431-5p overexpression on cell viability, but cell death occurred earlier. This deviation could be linked to the stronger repression of *ATP6V0E1* by siRNA-mediated knockdown than by miRNA overexpression (approximately 90% vs. 60–70%, respectively). However, the underlying effects of a miRNA should be interpreted with caution, as a single miRNA can regulate several hundreds of different gene transcripts (Friedman et al., 2009). The biological function of a miRNA therefore depends on the interplay of the total number of genes it affects. It is possible that some of the target genes of miR-431-5p have opposing effects on cell viability until the anti-proliferative and apoptotic effects become dominant and irreversible.

It is believed that the composition of subunit isoforms affects the activity and localization of V-ATPases (Stransky et al., 2016). However, little is known about subunit e of the $V_0$ domain, and its function is unclear, as removal of the subunit by detergent does not affect enzyme activity *in vitro* (Bueler and Rubinstein, 2015). As the authors discuss, this does not exclude its necessity for enzyme activity *in vivo* or possible involvement in enzyme assembly. Studies in yeast (*Saccharomyces cerevisiae*) have shown that the loss of subunit e prevents vacuole acidification (Davis-Kaplan et al., 2004; Sambade and Kane, 2004), which is probably due to a lack of $V_0$ domain assembly in the endoplasmic reticulum (Compton et al., 2006). We do not have evidence that a similar scenario occurs in the BxPC-3 cells, but it is plausible. Nonetheless, this is to our knowledge the first time a functional role has been reported for V-ATPase subunit e outside yeast.

PDAC cell lines as a model for PDAC may have limitations by not adequately represent primary cells and the heterogeneity of the tumour microenvironment. Thus, care should be taken when extrapolating the findings to the situation *in vivo*. However, cell lines are easier to manipulate (e.g. transfections) and enables reproducible experiments on the same cellular background, which are valuable properties when studying novel regulatory mechanisms, such as miRNA-mediated repression. Many studies on miRNA function, including ours, involve overexpressing the miRNA of interest with a mimic. A limitation to this approach is the supraphysiological levels reached, which could lead to excessive repression of target genes that would otherwise remain functional (Vidigal and Ventura, 2015). Nevertheless, identifying gene targets can be difficult without overexpressing the miRNA in question. Also, the use of miRNA mimics can serve as a useful approach for identifying miRNAs that have therapeutic potential (Setten et al., 2019). The expression of *HCAR1* and *ATP6V0E1* was only studied at the mRNA level, since we did not have access to specific antibodies of good quality.

In summary, we demonstrate that the lactate receptor HCAR1 is a target of miR-431-5p, and that their expression levels seem to be negatively related in the PDAC cell lines BxPC-3, Capan-2, and PANC-1. Overexpressing miR-431-5p inhibits proliferation in all the cell lines and induces apoptosis in BxPC-3 cells. The effects of miR-431-5p overexpression is likely to be a result of many affected genes involved in cancer-related processes and signalling pathways, as revealed by mRNA-Seq. One of the most significantly repressed genes was *ATP6V0E1*, encoding subunit e of V-ATPase, and knockdown of *ATP6V0E1* mimicked the effect of miR-431-5p overexpression on cell viability in BxPC-3 cells. We therefore believe that *ATP6V0E1* repression is a key contributor to the effects of miR-431-5p overexpression, although the underlying mechanism remains to be elucidated. It would also be of interest to further elucidate the clinical relevance of miR-431-5p in patients with PDAC, which would substantiate our findings of this miRNA as a tumour suppressor and a potential biomarker and/or therapeutic tool.

## 4. Materials and methods

### 4.1. Cell culture

BxPC-3 (ATCC® CRL1687™) and HEK-293T (ATCC® CRL-3216™) cells were purchased from ATCC. Capan-2 (ATCC® HTB-80™) and PANC-1 (ATCC® CRL-1469™) cells were kindly provided by Dr. Manoj Amrutkar and Dr. Hans-Christian Åsheim (University of Oslo, Norway). BxPC-3 cells were cultured in GlutaMAX-supplemented RPMI 1640 medium (Gibco), whereas Capan-2, PANC-1, and HEK-293T cells were cultured in L-glutamine-containing DMEM (Sigma-Aldrich). Complete growth medium was supplemented with 10% fetal bovine serum and Antibiotic-Antimycotic (Gibco) (100 U/ml penicillin, 100 µg/ml streptomycin, 0.25 µg/ml amphotericin B). The cells were kept in a humidified culture chamber with 5% $CO_2$ atmosphere at 37 °C. The growth medium was changed 2–3 times per week, and the cells were subcultured by trypsinization before reaching complete confluence. All experiments were performed within passage 15 after thawing of the original stock.

### 4.2. miRNA target prediction

TargetScanHuman (v7.2) was used to search for potential miRNAs that could be targeting *HCAR1* transcripts. TargetScan considers site type and 14 additional features to predict the most effectively targeted mRNAs (Agarwal et al., 2015).

### 4.3. Transfection

Cells were reverse-transfected with Lipofectamine RNAiMAX (Invitrogen) and 10 nM miRNA mimic or 5 nM small interfering RNA (siRNA), depending on the experiment. An equal concentration of All-Stars Negative Control siRNA was used as a negative control (QIAGEN), which is QIAGEN's validated negative control for siRNA and miRNA mimic experiments. hsa-miR-431-5p mimic (C-300729-03-0005) was purchased from Dharmacon, and TriFECTa DsiRNA Kit for *ATP6V0E1* (hs.Ri.ATP6V0E1.13) and *HCAR1* (hs.Ri.HCAR1.13) were purchased from Integrated DNA Technologies. 2 µl lipofectamine was used per final volume of 1.1 ml growth medium in a 12-well plate format and was scaled up or down based on the well size used for an experiment. At the start of transfection, the Antibiotic-Antimycotic was removed and the fetal bovine serum was reduced to 5%. The cells were cultured in complete growth medium from the following day.

### 4.4. RNA isolation

Transfected cells were harvested by trypsinization and centrifugation. Total RNA was isolated with RNeasy Mini Kit (QIAGEN), and miRNA was isolated with mirPremier microRNA Isolation Kit (Sigma-Aldrich), according to the manufacturers' instructions. Isolated RNA was DNase-treated with TURBO DNA-free kit (Invitrogen) to remove any residual genomic DNA. Concentration and purity were assessed with a NanoDrop ND-1000 spectrophotometer (Thermo Scientific).

### 4.5. cDNA synthesis and qPCR

Total RNA (400 ng) was used as input per 20 µl cDNA reaction mixture with Reverse Transcriptase Core Kit (Eurogentec). cDNA (50 ng) was then used as template for qPCR with Takyon Low ROX Probe MasterMix dTTP Blue (Eurogentec). The qPCR thermal profile consisted of an activation step at 95 °C for 3 min, followed by 40 cycles of denaturation at 95 °C for 10 sec, and annealing/extension at 60 °C for 1 min.

Isolated miRNA (10 ng) was used as input for cDNA synthesis with TaqMan™ Advanced miRNA cDNA Synthesis Kit (Applied Biosystems) according to the manufacturer's instructions. Briefly, mature miRNAs were polyadenylated at the 3′ end and extended at the 5′ end by adaptor ligation. The modified miRNAs then underwent reverse transcription, followed by amplification to uniformly increase the cDNA for all the miRNAs. The final product was diluted 1:10, and 5 µl was used as template for qPCR with TaqMan™ Fast Advanced Master Mix (Applied Biosystems). The qPCR thermal profile consisted of an activation step at

95 °C for 20 sec, followed by 40 cycles of denaturation at 95 °C for 3 sec, and annealing/extension at 60 °C for 30 sec.

Pre-designed TaqMan primer probes (Applied Biosystems) were used to analyze the expression of the genes and miRNAs of interest. *TBP* and hsa-miR-423-3p were used as reference genes for normalization. All reactions were run in triplicates together with no template controls on an AriaMx Real-Time PCR System (Agilent Technologies). The comparative threshold cycle ($2^{-\Delta\Delta Ct}$) method was used to calculate the relative gene expression (Livak and Schmittgen, 2001), with the expression for the reference group set to 1.

### 4.6. mRNA-Seq

Total RNA from BxPC-3 cells transfected with hsa-miR-431-5p mimic, isolated from three independent experiments (biological triplicates), was sent to Novogene for mRNA-Seq and subsequent analysis. The procedures performed by Novogene are briefly described here. Possible RNA degradation was examined on a 1% agarose gel, and RNA integrity was assessed on an Agilent 2100 Bioanalyzer. Total RNA (1 μg) per sample was used as the starting material for RNA sample preparations. Sequencing libraries were generated using NEB Next® Ultra™ RNA Library Prep Kit for Illumina® (NEB) according to the manufacturer's instructions. Briefly, mRNA was enriched using oligo$(dT)_{25}$ magnetic beads, fragmented, and converted to double-stranded cDNA. After sequencing adapter ligation, the cDNA was PCR-amplified, and index codes were added to attribute sequences to each sample. The PCR products were purified, and library quality, insert size, and concentration were assessed on a Qubit 2.0 Fluorometer (Life Technologies), an Agilent 2100 Bioanalyzer, and by qPCR. Following cluster generation of index-coded samples, the library preparations were sequenced on an Illumina HiSeq platform, generating 150-bp paired-end reads.

### 4.7. mRNA-Seq data analysis

Raw reads were filtered by removing reads with adapter contamination, ambiguous bases, and low-quality reads. The clean reads were mapped to the human reference genome GRCh38.p3 using TopHat v2.0.12. The number of reads mapped to each gene in the reference genome were counted with HTSeq software using the union mode. The FPKM (fragments per kilobase of transcript per million fragments mapped) was calculated to normalize the read counts by taking into account the gene length and the sequencing depth (Trapnell et al., 2010). An FPKM value of 1 was set as the threshold for determining whether the gene was expressed or not. Differentially expressed genes (DEGs) were calculated with the DESeq package in R, which uses a negative binomial distribution model. The resulting P-values were adjusted for false positives with the Benjamini-Hochberg method ($P_{adj} < 0.05$) (Benjamini and Hochberg, 1995). Gene Ontology (GO) term enrichment analysis of DEGs was performed using GOseq software (Young et al., 2010), and Kyoto Encyclopedia of Genes and Genomes (KEGG) pathway enrichment analysis of DEGs was performed with KOBAS software (Mao et al., 2005).

### 4.8. Cell counting

Cells (125 000 per well) were reverse-transfected in 12-well plates. After 24, 48, and 72 h, the cells were trypsinized and resuspended in equal volumes of growth medium before being counted by using a MOXI Z Mini Automated Cell Counter (ORFLO).

### 4.9. Western blot

Transfected cells were washed with ice-cold phosphate-buffered saline (PBS) and scraped in ice-cold radioimmunoprecipitation assay (RIPA) buffer containing Halt™ Protease and Phosphatase Inhibitor Cocktail (Thermo Scientific). The lysate was collected in pre-cooled Eppendorf tubes and mechanically homogenized by being passed repeatedly through a 29-gauge syringe (BD Micro-Fine). The lysate was then centrifuged at 16 000*g* in a 4 °C precooled centrifuge for 20 min, and the supernatant was transferred to new precooled microcentrifuge tubes. The protein concentration was determined with the Pierce™ BCA Protein Assay Kit (Thermo Scientific) according to the manufacturer's protocol. Then, Laemmli buffer and 50 mM dithiothreitol (DTT) were added to the samples, and boiled for 5 min at 95 °C.

Protein (30 μg) was separated on a polyacrylamide gel (4569033, Bio-Rad) and subsequently transferred to a 0.45-μm pore size nitrocellulose membrane with a Trans-Blot® Turbo™ Transfer System (Bio-Rad). The membrane was blocked with 5% milk in Tris-buffered saline with Tween 20 (TBST) at room temperature and incubated with primary antibody overnight at 4 °C. The primary antibodies used were: anti-phospho-Akt (Ser473) (4060, Cell Signaling, 1:2000), anti-Akt (4691, Cell Signaling, 1:2000), anti-Cdc42 (cell division cycle 42) (MAB3707, Chemicon, 1:1000), anti-PARP1 [poly(ADP-ribose) polymerase 1] (ab32138, Abcam, 1:1000), anti-Survivin (ab76424, Abcam, 1:20 000) and anti-GAPDH (ab9484, Abcam, 1:10 000). The membrane was then washed 3 × 10 min in TBST, incubated with horseradish peroxidase (HRP)-conjugated species-specific secondary antibody (Amersham ECL Rabbit IgG (NA934) or Mouse IgG (NA931), GE Healthcare, 1:20 000) for 1 h at room temperature and washed 3 × 10 min again in TBST. Finally, the membrane was incubated for 5 min in the dark with ECL substrate (1705060, Bio-Rad), and images were acquired with a ChemiDoc™ Touch Imaging System (Bio-Rad). After probing the membrane with phospho-Akt antibody, the membrane was stripped and re-probed with total Akt antibody.

### 4.10. Cell cycle analysis

Cell cycle progression was assessed using NUCLEAR-ID® Green Cell Cycle Kit (Enzo Life Sciences). Cells treated with 50 ng/ml nocodazole for 24 h were used as a positive control. After 48 h, the transfected cells were harvested, and cell pellets were resuspended in a small volume of PBS. For fixation, 5 ml 70% ice cold ethanol (−20 °C) was added dropwise to the cells with ongoing shaking to prevent clumping. The cells were then incubated at 4 °C for 30 min. Prior to DNA staining, the fixed cells were centrifuged, followed by removal of fixative, and washed with 1X assay buffer. After a final centrifugation and supernatant removal, the cells were resuspended in freshly made 20 μM DNA Staining Solution and incubated in the dark at 37 °C for 30 min. The cells were analyzed in the FL1 (green) channel of a FACSCalibur flow cytometer (Becton Dickinson), and the data were analyzed with Flowing Software (flowingsoftware.btk.fi).

### 4.11. Apoptosis assay

Transfected cells were harvested for the apoptosis assay using Single Channel Annexin V/Dead Cell Apoptosis Kit (Invitrogen). Briefly, after centrifugation and supernatant removal, the cells were resuspended in 100 μl 1X annexin binding buffer, to which 5 μl Alexa Fluor® 488 annexin V and 1 μl 5 μM SYTOX® Green working solution were added. The cells were then incubated in the dark at 37 °C for 30 min, and 400 μl 1X annexin binding buffer was added after incubation. The cells were analyzed in the FL1 (green) channel of a FACSCalibur flow cytometer, and the data were analyzed with ImageJ software.

### 4.12. 3′ UTR dual-reporter assay

Dual-reporter constructs for the three prime untranslated region (3′ UTR) of *HCAR1* (HmiT127367-MT05) and *ATP6V0E1* (HmiT127368-MT05) were obtained from GeneCopoeia. These are constructed from the pEZX-MT05 vector (CmiT000001-MT05), which encodes a secreted Gaussian Luciferase (GLuc) and a secreted Alkaline Phosphatase (SEAP), and contain the 3′ UTR sequence of either *HCAR1* or *ATP6V0E1*

downstream of the GLuc gene. Binding of miRNA to the 3′ UTR of the chimeric GLuc mRNA will decrease the expression of secreted GLuc. The expression of SEAP is unaffected and serves as an internal control.

HEK-293 T cells ($1.25 \times 10^5$ cells per well in a 24-well format) were reverse-transfected with 10 nM miR-431-5p mimic or AllStars Negative Control siRNA (QIAGEN) using 1 ul Lipofectamine RNAiMAX reagent (Invitrogen). 24 h later, the cells were re-transfected with 500 ng dual-reporter construct using 1 ul Lipofectamine 3000 reagent and 1 ul P3000 reagent (Invitrogen). The culture medium was replaced with complete growth medium the following day, and the cells were left in culture for 48 h prior to collection of culture medium. The Secrete-Pair™ Dual Luminescence Assay Kit (GeneCopoeia) was used to prepare the collected samples for the measure of GLuc and SEAP activities, in accordance with the manufacturer's instructions. Luminescence was measured in a white 96-well plate in a Cytation 3 microplate reader (BioTek). The GLuc activity was normalized to the SEAP activity to account for variations in cell numbers.

### 4.13. Statistical analysis

Statistical analysis of functional experiments was performed using paired *t*-test in GraphPad Prism version 8.0. $P < 0.05$ was considered statistically significant.

## 5. Data availability statement

The datasets generated during and/or analysed during the current study are available in the

European Nucleotide Archive (ENA) at EMBL-EBI under accession number PRJEB40486.

## Declaration of Competing Interest

The authors declare that they have no known competing financial interests or personal relationships that could have appeared to influence the work reported in this paper.

### Acknowledgements

We would like to thank Dr. Manoj Amrutkar (Institute of Clinical Medicine, Faculty of Medicine, University of Oslo) for having provided us with the Capan-2 cell line, and Dr. Hans-Christian Åsheim (Institute of Oral Biology, Faculty of Dentistry, University of Oslo), who provided us with the PANC-1 cell line. The study was funded by the Institute of Oral Biology (University of Oslo) and the Department of Medical Biochemistry (Oslo University Hospital).

### Author contributions

ØPH and LHB were responsible for the study conception. ØPH was responsible for and CK contributed to methodology, data acquisition, analyses, and interpretation. HMW and TPU contributed to the data acquisition. ØPH wrote the manuscript, and all authors critically revised and approved the final manuscript.

## Appendix A. Supplementary data

Supplementary data to this article can be found online at https://doi.org/10.1016/j.gene.2022.146346.

## References

Agarwal, V., Bell, G.W., Nam, J.-W., Bartel, D.P., 2015. Predicting effective microRNA target sites in mammalian mRNAs. Elife 4. https://doi.org/10.7554/eLife.05005.

Bartel, D.P., 2018. Metazoan MicroRNAs. Cell 173 (1), 20–51. https://doi.org/10.1016/j.cell.2018.03.006.

Benjamini, Y., Hochberg, Y., 1995. Controlling the False Discovery Rate: A Practical and Powerful Approach to Multiple Testing. J. Roy. Stat. Soc.: Ser. B (Methodol.) 57 (1), 289–300. https://doi.org/10.1111/j.2517-6161.1995.tb02031.x.

Bray, F., Ferlay, J., Soerjomataram, I., Siegel, R.L., Torre, L.A., Jemal, A., 2018. Global cancer statistics 2018: GLOBOCAN estimates of incidence and mortality worldwide for 36 cancers in 185 countries. CA Cancer J. Clin. 68 (6), 394–424. https://doi.org/10.3322/caac.21492.

Bryant, K.L., Mancias, J.D., Kimmelman, A.C., Der, C.J., 2014. KRAS: feeding pancreatic cancer proliferation. Trends Biochem. Sci. 39 (2), 91–100. https://doi.org/10.1016/j.tibs.2013.12.004.

Bueler, S.A., Rubinstein, J.L., 2015. Vma9p need not be associated with the yeast V-ATPase for fully-coupled proton pumping activity in vitro. Biochemistry 54 (3), 853–858. https://doi.org/10.1021/bi5013172.

Chen, S.-H., Zhang, Y., Van Horn, R.D., Yin, T., Buchanan, S., Yadav, V., Mochalkin, I., Wong, S.S., Yue, Y.G., Huber, L., Conti, I., Henry, J.R., Starling, J.J., Plowman, G.D., Peng, S.-B., 2016. Oncogenic BRAF Deletions That Function as Homodimers and Are Sensitive to Inhibition by RAF Dimer Inhibitor LY3009120. Cancer Discov. 6 (3), 300–315.

Compton, M.A., Graham, L.A., Stevens, T.H., 2006. Vma9p (subunit e) is an integral membrane V0 subunit of the yeast V-ATPase. J. Biol. Chem. 281 (22), 15312–15319. https://doi.org/10.1074/jbc.M600890200.

Damaghi, M., Wojtkowiak, J.W., Gillies, R.J., 2013. pH sensing and regulation in cancer. Front. Physiol. 4, 370. https://doi.org/10.3389/fphys.2013.00370.

Davis-Kaplan, S.R., Ward, D.M., Shiflett, S.L., Kaplan, J., 2004. Genome-wide analysis of iron-dependent growth reveals a novel yeast gene required for vacuolar acidification. J. Biol. Chem. 279 (6), 4322–4329. https://doi.org/10.1074/jbc.M310680200.

Deer, E.L., González-Hernández, J., Coursen, J.D., Shea, J.E., Ngatia, J., Scaife, C.L., Firpo, M.A., Mulvihill, S.J., 2010. Phenotype and genotype of pancreatic cancer cell lines. Pancreas 39 (4), 425–435. https://doi.org/10.1097/MPA.0b013e3181c15963.

Erkan, M., Kurtoglu, M., Kleeff, J., 2016. The role of hypoxia in pancreatic cancer: a potential therapeutic target? Expert Rev. Gastroenterol. Hepatol. 10 (3), 301–316. https://doi.org/10.1586/17474124.2016.1117386.

Friedman, R.C., Farh, K.K., Burge, C.B., Bartel, D.P., 2009. Most mammalian mRNAs are conserved targets of microRNAs. Genome Res. 19 (1), 92–105. https://doi.org/10.1101/gr.082701.108.

Fruman, D.A., Chiu, H., Hopkins, B.D., Bagrodia, S., Cantley, L.C., Abraham, R.T., 2017. The PI3K Pathway in Human Disease. Cell 170 (4), 605–635. https://doi.org/10.1016/j.cell.2017.07.029.

Grimson, A., Farh, K.K., Johnston, W.K., Garrett-Engele, P., Lim, L.P., Bartel, D.P., 2007. MicroRNA targeting specificity in mammals: determinants beyond seed pairing. Mol. Cell 27 (1), 91–105. https://doi.org/10.1016/j.molcel.2007.06.017.

Guillaumond, F., Leca, J., Olivares, O., Lavaut, M.-N., Vidal, N., Berthezene, P., Dusetti, N.J., Loncle, C., Calvo, E., Turrini, O., Iovanna, J.L., Tomasini, R., Vasseur, S., 2013. Strengthened glycolysis under hypoxia supports tumor symbiosis and hexosamine biosynthesis in pancreatic adenocarcinoma. Proc. Natl. Acad. Sci. U S A 110 (10), 3919–3924. https://doi.org/10.1073/pnas.1219555110.

Kennedy, K.M., Scarbrough, P.M., Ribeiro, A., Richardson, R., Yuan, H., Sonveaux, P., Landon, C.D., Chi, J.-T., Pizzo, S., Schroeder, T., Dewhirst, M.W., Moreno-Sanchez, R., 2013. Catabolism of exogenous lactate reveals it as a legitimate metabolic substrate in breast cancer. PLoS ONE 8 (9), e75154. https://doi.org/10.1371/journal.pone.0075154.

Kleeff, J., Korc, M., Apte, M., La Vecchia, C., Johnson, C.D., Biankin, A.V., Neale, R.E., Tempero, M., Tuveson, D.A., Hruban, R.H., Neoptolemos, J.P., 2016. Pancreatic cancer. Nat. Rev. Dis. Primers 2 (1). https://doi.org/10.1038/nrdp.2016.22.

Kong, Q., Han, J., Deng, H., Wu, F., Guo, S., Ye, Z., 2018. miR-431-5p alters the epithelial-to-mesenchymal transition markers by targeting UROC28 in hepatoma cells. Onco Targets Ther. 11, 6489–6503. https://doi.org/10.2147/ott.S173840.

Li, M.-F., Li, Y.-H., He, Y.-H., Wang, Q., Zhang, Y., Li, X.-F., Meng, X.-M., Huang, C., Li, J., 2018. Emerging roles of hsa_circ_0005075 targeting miR-431 in the progress of HCC. Biomed. Pharmacother. 99, 848–858. https://doi.org/10.1016/j.biopha.2018.01.150.

Livak, K.J., Schmittgen, T.D., 2001. Analysis of relative gene expression data using real-time quantitative PCR and the 2(-Delta Delta C(T)) Method. Methods 25 (4), 402–408. https://doi.org/10.1006/meth.2001.1262.

Mao, X., Cai, T., Olyarchuk, J.G., Wei, L., 2005. Automated genome annotation and pathway identification using the KEGG Orthology (KO) as a controlled vocabulary. Bioinformatics 21 (19), 3787–3793. https://doi.org/10.1093/bioinformatics/bti430.

Massihnia, D., Avan, A., Funel, N., Maftouh, M., van Krieken, A., Granchi, C., Raktoe, R., Boggi, U., Aicher, B., Minutolo, F., Russo, A., Leon, L.G., Peters, G.J., Giovannetti, E., 2017. Phospho-Akt overexpression is prognostic and can be used to tailor the synergistic interaction of Akt inhibitors with gemcitabine in pancreatic cancer. J. Hematol. Oncol. 10 (1) https://doi.org/10.1186/s13045-016-0371-1.

Morimura, T., Fujita, K., Akita, M., Nagashima, M., Satomi, A., 2008. The proton pump inhibitor inhibits cell growth and induces apoptosis in human hepatoblastoma. Pediatr. Surg. Int. 24 (10), 1087–1094. https://doi.org/10.1007/s00383-008-2229-2.

Nakashima, S., Hiraku, Y., Tada-Oikawa, S., Hishita, T., Gabazza, E.C., Tamaki, S., Kawanishi, S., 2003. Vacuolar H+-ATPase inhibitor induces apoptosis via lysosomal dysfunction in the human gastric cancer cell line MKN-1. J. Biochem. 134 (3), 359–364. https://doi.org/10.1093/jb/mvg153.

Olson, M.F., Ashworth, A., Hall, A., 1995. An essential role for Rho, Rac, and Cdc42 GTPases in cell cycle progression through G1. Science 269 (5228), 1270–1272. https://doi.org/10.1126/science.7652575.

Pérez-Escuredo, J., Van Hée, V.F., Sboarina, M., Falces, J., Payen, V.L., Pellerin, L., Sonveaux, P., 2016. Monocarboxylate transporters in the brain and in cancer. BBA 1863 (10), 2481–2497. https://doi.org/10.1016/j.bbamcr.2016.03.013.

Polireddy, K., Chen, Q., 2016. Cancer of the Pancreas: Molecular Pathways and Current Advancement in Treatment. J. Cancer 7 (11), 1497–1514. https://doi.org/10.7150/jca.14922.

Rahib, L., Smith, B.D., Aizenberg, R., Rosenzweig, A.B., Fleshman, J.M., Matrisian, L.M., 2014. Projecting cancer incidence and deaths to 2030: the unexpected burden of thyroid, liver, and pancreas cancers in the United States. Cancer Res. 74 (11), 2913–2921. https://doi.org/10.1158/0008-5472.Can-14-0155.

Rapa, I., Votta, A., Felice, B., Righi, L., Giorcelli, J., Scarpa, A., Speel, E.-J., Scagliotti, G. V., Papotti, M., Volante, M., 2015. Identification of MicroRNAs Differentially Expressed in Lung Carcinoid Subtypes and Progression. Neuroendocrinology 101 (3), 246–255. https://doi.org/10.1159/000381454.

Roland, C.L., Arumugam, T., Deng, D., Liu, S.H., Philip, B., Gomez, S., Burns, W.R., Ramachandran, V., Wang, H., Cruz-Monserrate, Z., Logsdon, C.D., 2014. Cell surface lactate receptor GPR81 is crucial for cancer cell survival. Cancer Res 74 (18), 5301–5310.

Rupaimoole, R., Slack, F.J., 2017. MicroRNA therapeutics: towards a new era for the management of cancer and other diseases. Nat. Rev. Drug Discov. 16 (3), 203–222. https://doi.org/10.1038/nrd.2016.246.

Sambade, M., Kane, P.M., 2004. The yeast vacuolar proton-translocating ATPase contains a subunit homologous to the Manduca sexta and bovine e subunits that is essential for function. J. Biol. Chem. 279 (17), 17361–17365. https://doi.org/10.1074/jbc.M314104200.

Schultz, N.A., Andersen, K.K., Roslind, A., Willenbrock, H., Wøjdemann, M., Johansen, J. S., 2012. Prognostic microRNAs in cancer tissue from patients operated for pancreatic cancer–five microRNAs in a prognostic index. World J. Surg. 36 (11), 2699–2707. https://doi.org/10.1007/s00268-012-1705-y.

Setten, R.L., Rossi, J.J., Han, S.P., 2019. The current state and future directions of RNAi-based therapeutics. Nat. Rev. Drug Discov. 18 (6), 421–446. https://doi.org/10.1038/s41573-019-0017-4.

Siegel, R.L., Miller, K.D., Jemal, A., 2020. Cancer statistics, 2020. CA Cancer J. Clin. 70 (1), 7–30. https://doi.org/10.3322/caac.21590.

Sonveaux, P., Végran, F., Schroeder, T., Wergin, M.C., Verrax, J., Rabbani, Z.N., et al., 2008. Targeting lactate-fueled respiration selectively kills hypoxic tumor cells in mice. The Journal of clinical investigation, 118(12), 3930-3942. doi:10.1172/JCI36843.

Stransky, L., Cotter, K., Forgac, M., 2016. The Function of V-ATPases in Cancer. Physiol. Rev. 96 (3), 1071–1091. https://doi.org/10.1152/physrev.00035.2015.

Sun, K., Zeng, T., Huang, D., Liu, Z., Huang, S., Liu, J., Qu, Z., 2015. MicroRNA-431 inhibits migration and invasion of hepatocellular carcinoma cells by targeting the ZEB1-mediated epithelial-mensenchymal transition. FEBS Open Bio 5, 900–907. https://doi.org/10.1016/j.fob.2015.11.001.

Trapnell, C., Williams, B.A., Pertea, G., Mortazavi, A., Kwan, G., van Baren, M.J., Salzberg, S.L., Wold, B.J., Pachter, L., 2010. Transcript assembly and quantification by RNA-Seq reveals unannotated transcripts and isoform switching during cell differentiation. Nat. Biotechnol 28 (5), 511–515. https://doi.org/10.1038/nbt.1621.

Vidigal, J.A., Ventura, A., 2015. The biological functions of miRNAs: lessons from in vivo studies. Trends Cell Biol. 25 (3), 137–147. https://doi.org/10.1016/j.tcb.2014.11.004.

von Schwarzenberg, K., Wiedmann, R.M., Oak, P., Schulz, S., Zischka, H., Wanner, G., Efferth, T., Trauner, D., Vollmar, A.M., 2013. Mode of cell death induction by pharmacological vacuolar H+-ATPase (V-ATPase) inhibition. J. Biol. Chem. 288 (2), 1385–1396. https://doi.org/10.1074/jbc.M112.412007.

Xie, Q., Zhu, Z., He, Y., Zhang, Z., Zhang, Y., Wang, Y., Luo, J., Peng, T., Cheng, F., Gao, J., Cao, Y., Wei, H., Wu, Z., 2020. A lactate-induced Snail/STAT3 pathway drives GPR81 expression in lung cancer cells. Biochim. Biophys. Acta Mol. Basis Dis. 1866 (1), 165576. https://doi.org/10.1016/j.bbadis.2019.165576.

Yang, J., Zhu, H., Jin, Y., Song, Y., 2018. MiR-431 inhibits cell proliferation and induces cell apoptosis by targeting CDK14 in pancreatic cancer. Eur. Rev. Med. Pharmacol. Sci. 22 (14), 4493–4499. https://doi.org/10.26355/eurrev_201807_15503.

Young, M.D., Wakefield, M.J., Smyth, G.K., Oshlack, A., 2010. Gene ontology analysis for RNA-seq: accounting for selection bias. Genome Biol. 11 (2), R14. https://doi.org/10.1186/gb-2010-11-2-r14.

Yuen, A., Díaz, B., 2014. The impact of hypoxia in pancreatic cancer invasion and metastasis. Hypoxia (Auckl) 2, 91–106. https://doi.org/10.2147/hp.S52636.